International Journal of Plant & Soil Science

32(13): 13-33, 2020; Article no.IJPSS.61263
ISSN: 2320-7035

Modelling and Delineation of Hydrocarbon Micro - Seepage Prone Zones on Soil and Sediment in Ugwueme, South Eastern Nigeria with Soil Adjustment Vegetation Index (SAVI)

Mfoniso Asuquo Enoh[1*], Uzoma Chinenye Okeke[2] and Needam Yiinu Barinua[3]

[1]Department of Geoinformatics and Surveying, Faculty of Environmental Studies, University of Nigeria, Nigeria.
[2]Department of Surveying and Geoinformatics, Faculty of Environmental Sciences, Nnamdi Azikiwe University, Awka, Nigeria.
[3]Department of Surveying and Geoinformatics, Ken Polytechnic Bori, Rivers State, Nigeria.

Authors' contributions

This work was carried out in collaboration among all authors. Authors MAE, UCO and NYB designed the study, performed the statistical analysis, wrote the protocol and the first draft of the manuscript. Authors MAE, UCO and NYB managed the analyses of the study and the literature searches. All authors read and approved the final manuscript.

Article Information

DOI: 10.9734/IJPSS/2020/v32i1330355
Editor(s):
(1) Marco Trevisan, Catholic University of the Sacred Heart, Italy.
Reviewers:
(1) Abhay Kumar Soni, CSIR-Central Institute of Mining and Fuel Research (CSIR-CIMFR), India.
(2) Arvind Lal, Central University of Jharkhand, India.
Complete Peer review History: http://www.sdiarticle4.com/review-history/61263

Original Research Article

Received 20 July 2020
Accepted 24 September 2020
Published 19 October 2020

ABSTRACT

Remote Sensing is an excellent tool in monitoring, mapping and interpreting areas, associated with hydrocarbon micro-seepage. An important technique in remote sensing known as the Soil Adjusted Vegetation Index (SAVI), adopted in many studies is often used to minimize the effect of brightness reflectance in the Normalized Difference Vegetation Index (NDVI), related with soil in areas of spare vegetation cover, and mostly in areas of arid and semi–arid regions. The study aim at analyzing the effect of hydrocarbon micro – seepage on soil and sediments in Ugwueme, Southern Eastern Nigeria, with SAVI image classification method. To achieve this aim, three cloud free Landsat images, of Landsat 7 TM 1996 and ETM+ 2006 and Landsat 8 OLI 2016 were utilized to

**Corresponding author: E-mail: enohmfoniso@yahoo.com;*

produce different SAVI image classification maps for the study. The SAVI image classification analysis for the study showed three classes viz Low class cover, Moderate class cover and high class cover. The category of high SAVI density classification was observed to increase progressive from 31.95% in 1996 to 34.92% in 2006 and then to 36.77% in 2016. Moderately SAVI density classification reduced from 40.53% in 1996 to 38.77% in 2006 and then to 36.96% in 2016 while Low SAVI density classification decrease progressive from 27.51% in 1996 to 26.31% in 2006 and then increased to 28.26% in 2016. The SAVI model is categorized into three classes viz increase, decrease and unchanged. The un – changed category increased from 12.32km^2 (15.06%) in 1996 to 17.17 km^2 (20.96%) in 2006 and then decelerate to 13.50 km^2 (16.51%) in 2016. The decrease category changed from 39.89km^2 (48.78%) in 1996 to 40.45 km^2 (49.45%) in 2006 and to 51.52 km^2 (63.0%) in 2016 while the increase category changed from 29.57km^2 (36.16%) in 1996 to 24.18 km^2 (29.58%) in 2006 and to 16.75 km^2 (20.49%) in 2016. Image differencing, cross tabulation and overlay operations were some of the techniques performed in the study, to ascertain the effect of hydrocarbon micro - seepage. The Markov chain analysis was adopted to model and predict the effect of the hydrocarbon micro - seepage for the study for 2030. The study expound that the SAVI is an effective technique in remote sensing to identify, map and model the effect of hydrocarbon micro - seepage on soil and sediment particularly in areas characterized with low vegetation cover and bare soil cover.

Keywords: Hydrocarbon micro – seepage; remote sensing; SAVI; soil; sediment; Ugwueme.

1. INTRODUCTION

Underlying earth's reservoir are often saturated with hydrocarbon oil and gas. These reservoir permits the concealed oil and gas to escape, hence producing an oxidation – reduction which occur in situ or in nearly vertical direction, thereby emerging as micro - seepage at the earth's surface, and thus produce anomalies in overlying sediments and soils [1]. Hydrocarbon micro - seepage often contaminate the earth's surface soil and sediment, thereby influencing their stability, such that the form oxidation zone in the altered areas, hence the produce changes in their electrical and magnetic properties [2,3,4]. Hydrocarbon micro - seepage has a devastating effect on the soil and sediment. The effect is such that it produces a large range of changes within the soil environment, which depends on the type of soil; and the duration, which it influences the soil. The effect of hydrocarbon micro - seepage on the soil, also results in unusually high concentrations of ethane, propane and methane, thereby leading to mineral alterations as well as temperature, radiometric and geo – botanical anomalies [5]. Long term effect of hydrocarbon micro-seepage alters the mineral composition of soil and sediment, hence it produces a change in their chemical and physical properties, with evidence such as changes in color, hardness, electric, magnetic and radioactive properties of the soil and sediment minerals [5]. The impact of micro - seepage on overlying soil and sediment takes their constituents hydrophobic, but if the soil and sediment are properly managed, its effect will be minimal [6]. Anoliefo and Vwioko [7] opined that the presence of micro - seepage on the environment produces unsatisfactory atmosphere for plant growth, mainly due to their inability to aerate the soil. Noomen [8] stated that stress associated with plants arise owed to changes in the soil environment, hence micro - seepage often displace the soil air, resulting in oxygen shortage in the soil. The oxygen concentration in the soil may decrease further due to methanotrophic bacteria, which oxidize the methane which is present in natural oil and gas generating high concentration of carbon dioxide and water [9]. White [10] is of the view, that the soil structure viz pH, mineralogy and organic matter content may change, if they get in contact with hydrocarbon micro-seepage. Schumacher [4] quoted that hydrocarbon micro - seepage gas such as methane, ethane and carbon dioxide collect in the soil, often displace the normal soil atmosphere, which results in a decrease in the soil oxygen. These concentration of oxygen in the soil is noted to decrease further, as a result of methano – trophic bacteria, which oxidize methane, and in the process generate carbon dioxide and water [9].

Long term exposure of hydrocarbon micro - seepage on the soil and in the environment at large can produce a locally anomalous redox zones which aid the development of a diverse array of chemical and mineralogical changes [11]. Bacterial oxidation of micro - seepage can directly or indirectly generate changes in the pH

of the environment, which will influence the mineral stability and chemical reactivity of the soil [12]. According to the Petroleum Safety Authority [13], hydrocarbon micro - seepage promotes long term health issues, mainly due to high concentrations of toxic compounds [12]. If its effect is uncovered at an early stage, substantial volumes of explosive oil and gas in the soil, may generate into dangerous situation which involves costly remediation works [14]. The United States National Transportation Safety Board (NTSB) has highlight that millions of dollars is lost and several casualties reported, owing to the effect of oil and gas leaks on the soil [15,16]. Schumacher [17] quoted that the presence of hydrocarbon micro - seepage in the soil, often deplete soil oxygen and then produce stress to growing vegetation. White [10] stated that micro - seepages may influence vegetation in several ways. When they penetrate into plant system, it alter their metabolism and hence produce stress, which maybe visualize with signs such as stunted growth, yellowish leaves and poor yields [18]. Further impact of hydrocarbon micro - seepage on vegetation due to the soil, depends on varying factors, such as the type of soil to the life cycle development stage of the vegetation. Pysek and Pysek [19] equally noted that different vegetation types have varying sensitivity when they come in contact with seepages. National hydrocarbon seepage generate differs negative consequences on the environment and the society at large. The upwelling of tar and oil or "heavy hydrocarbon" consists mainly of greenhouse CO_2 and CH_4 and which give rise to local pollution of soil and water. Serrano *et al* [20] air his view that when hydrocarbon micro - seepage evolve at the earth's surface and into the soil, they persist in the soil, causing major deterioration to the soil physical properties as well as changes in microbes populations. Oil and gas seepage impacted soil may also cause alterations in the mineralogy of soil as well as in microbiological, biogeochemical and geo – botanical anomalies, which may be visible in the soil surface expression [4]. Several researchers have investigated on the use of spectroscopy in their study, to identify the impact of hydrocarbon micro - seepage on the soil [21,22,23,24]. The study of these researchers showed that there is an overall decrease in the reflectance properties of oil and gas impacted soil within the VIS – NIR (about 400 – 800 *nm*) wavelength regions and with conclusion that hydrocarbon micro-seepage have an absorption features in the 3.4μm, 2.35 μm, 1.75μm and 1.35μm wavelength region [24].

Schumacher [25] opined that the traditional methods for studying hydrocarbon micro - seepage is tedious, time consuming, destructive and expensive. Hence, remote sensing is an effective tool, which have been proven to be much more valid for interpreting and studying micro - seepage as the techniques offer a fast, non – destructive and less expensive method as compared to the traditional methods. Optical remote sensing have been utilized for exploring onshore hydrocarbon reservoirs, for the detection of hydrocarbons oil and gas seepage [22,26,23]. Ziring *et al* [27] opined that remote sensing is a new method for exploring oil and gas seepage detection. The Soil Adjusted vegetation Index (SAVI) is a remote sensing technique which is used to minimize the effect of brightness reflection in the Normalized Difference Vegetation Index (NDVI) that is caused by the soil [28]. The NDVI is a numerical indicator which utilize the visible and near – infrared bands of the electromagnetic spectrum, adopted to analyze remote sensing measurements and then assess if the target observed contains live green vegetation or not. The SAVI is an effective index, which is useful in areas with spare vegetation cover, such as arid and semi – arid regions. It is defined as follows:

$$\text{SAVI} = \frac{(1+L)\,(NIR - R)}{NIR + R + L}$$

Where: *NIR* is the near infrared reflectance*; R* is the red reflectance and *L* = 0.5, is an adjustment factor effective to minimize the backscatter effect of sol background reflectance through the canopy [29,30]. Spencer and Spry [31] opined that SAVI was proposed with the sole aim to minimize the effects of soil background on the quantification of greenness by a way to incorporate a soil adjustment factor (*L*) in the basic NDVI. Gibson *et al* [32] was also of the view that the (*L*) factor is determined by the relative percentage of vegetation and to state the nature of the soil (*L* = 0 for very high vegetation cover, *L* = 1 for very low vegetation cover and L = 0.5 for intermediate cover). SAVI is also viewed as an exponent, given to the red – band value in the denominator as well as multiplier (*L* = 1) of the associate first term.

This study depends on the soil adjustment vegetation index (SAVI) as a remote sensing technique to assess and interpret the effect of hydrocarbon micro-seepage on soil and sediment in Ugwueme, South Eastern Nigeria with dates of 1996, 2006 and 2016 for both image classification and the SAVI.

2. MATERIALS AND METHODS

2.1 The Study Area: Location and Accessibility

Ugwueme is situated on a hilly terrain, between Latitude 60 0 00 *N* and 60 07 00 *N* and Longitude 70 24 00 *E* and 70 30 00 *E* of geographical co – ordinates. The region is fairly populated and according to the latest population census conducted by the National Population Commission [33], the town has an estimated population of about 13,000 people. Ugwueme has accessible network of un – tarred and laterite graded road, which is often links farmlands, schools, worship places and markets. The study area is also linked to other parts of Eastern Nigeria, through the Ugwueme – Amadi road as well as the Enugu – Porthacourt dual express road [34]. Geologically, Ugwueme is underlain by iron stone beds with other sedimentary facies, which has attracted several tourists and other visitors to the area [35]. Many landforms exist in the area, and of which the major ones are the Cross River plain, Enugu Cuesta and Niger – Imo lowlands [36]. The Enugu – Awgu Cuesta is an asymmetrical ridge characterized with a long and dipping topography along the Western side of the scarp slope [36]. The Awgu Escarpment (cuesta) exist from a height ranging from 305*m* (1000ft) – 600*m* (2000ft) above the sea level. The lithology of Ugwueme is made up mostly of shale which is overlain by sandstone. Within the study area, the lowest area above sea level is 46*m* while the highest area is 600*m* [35]. Within the area, the soil type, called the Red Earth is conformed to the geological structure of the eastern part of Nigeria [37]. The Red Earth soil is characterized as shallows and stony lithosols, located on the topography of the cuesta [37]. Fig. 1 shows the political map of Ugwueme, while Fig. 2 present the soil map which is digitized from the soil map of Nigeria.

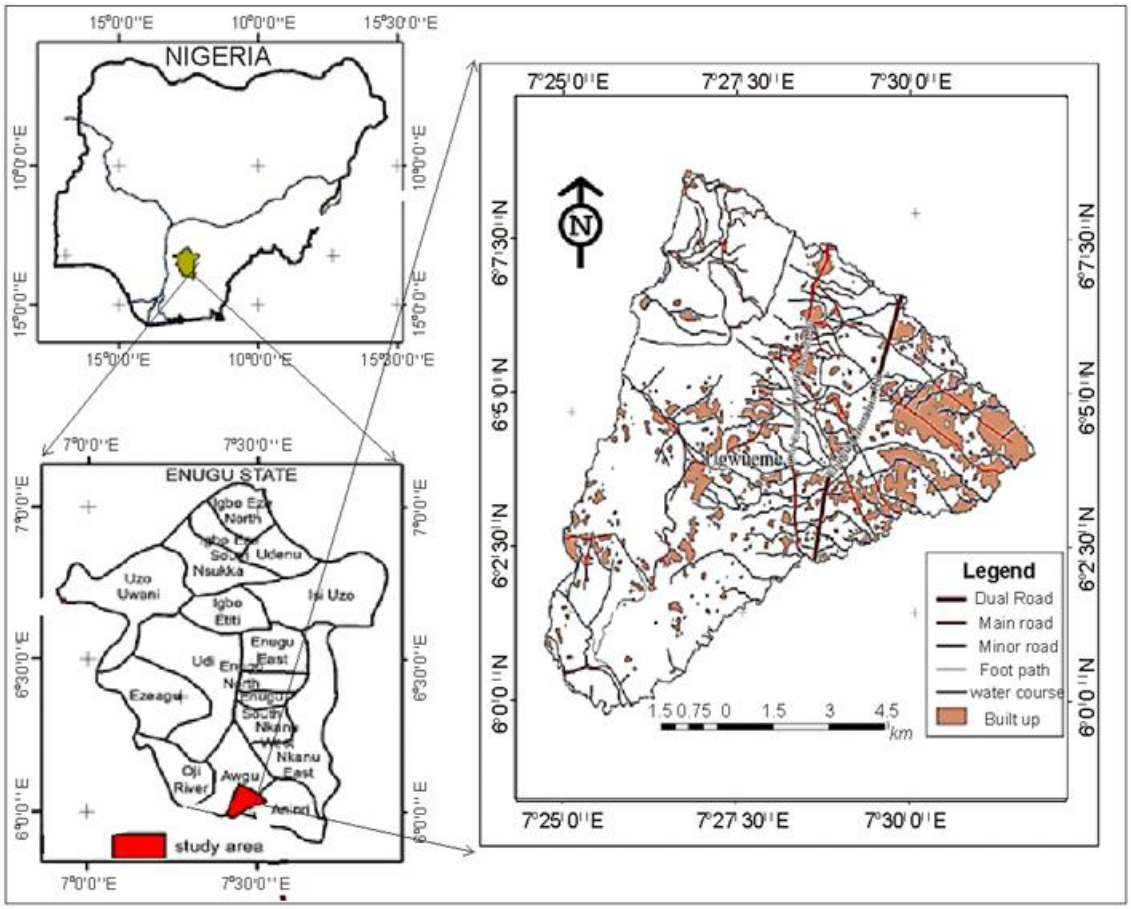

Fig. 1. Political map of Ugwueme

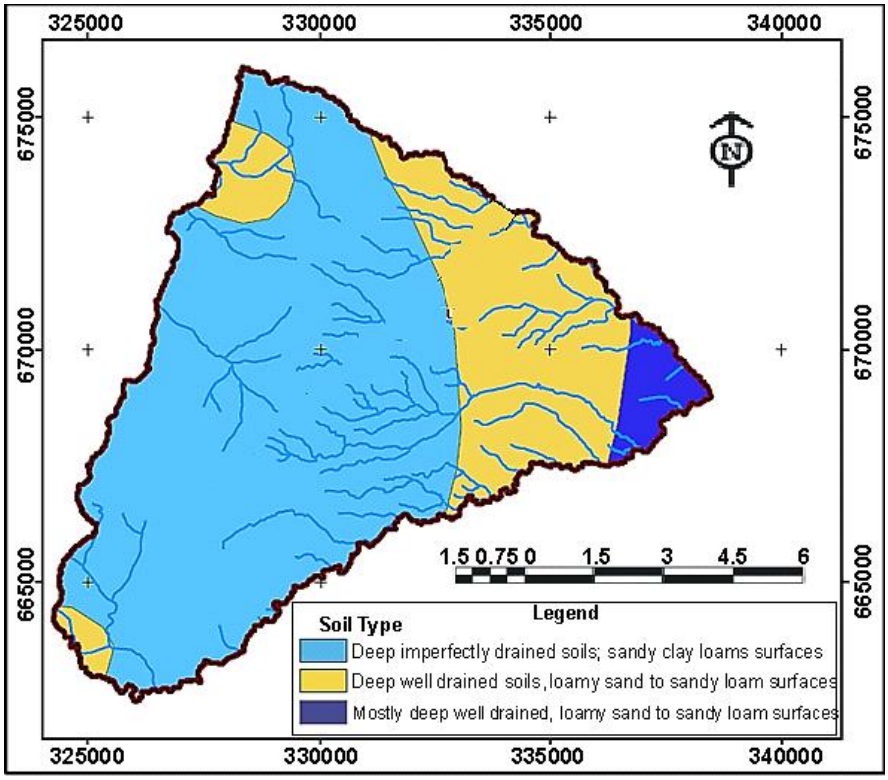

Fig. 2. Soil map of Ugwueme (digitized from the soil map of Nigeria)

2.2 Data Acquisition and Software

2.2.1 Primary data

Three cloud free imageries were derived freely at path 188 row 55 and 56 of Landsat 5 Thematic Mapper (*TM*) on 19th December 1996; Landsat 7 Enhanced Thematic Mapper plus (*ETM+*) on 17th December 2006 and Landsat 8 Operational Land Imager (OLI) on 25th January 2016 in a spatial resolution of 30m by 30m from the [38] website with Earth Explorer USGS.gov. The imageries were radio-metrically corrected with the United States Geological Service and then projected to Universal Transverse Mercator (UTM) zone 32 north of coordinate system available on the World Geodetic System (WGS) 1984 ellipsoid.

2.2.2 Secondary data

These data include the administrative, land use and topographic maps of Enugu urban. The Google Earth was also utilized to acquire the higher resolution images of the study area to aid accurate interpretation and classification of the satellite imageries and for accuracy assessment and modelling of the Landsat images used. The administrative map of the study, was utilized for creating the study area shape file, used to subset the Landsat images. This had an advantage, as the data sizes is reduced and the computer storage space decreased.

2.3 Software Used

The software adopted for the study are majorly, the ArcGIS 10.5, ERDAS Imagine 14.0 and the Idrisi Selva. The ERDAS Imagine software was utilized for layer stacking and to generate the false color composite (FCC), image co – registration, image sub – setting and classification. The ArcGIS software was adopted for addition of the images, attributes to data, for mosaicking of the respective scenes of Landsat imageries, to perform image overlay, as well as to determine the soil adjusted vegetative index (SAVI). The Idrisi Selva was used for the prediction analysis.

2.4 Remote Sensing Processes

Landsat Thematic Mapper (*TM*) and Enhanced Thematic Mapper plus (ETM+) sensors often capture solar energy, which reflects and then

convert the data to radiance, after which it rescale the data to a digital number (DN), which is 8 bit and ranges with values from 0 and 255. DNs can also be converted to ToA reflectance, manually with a two steps process. The first step involves converting the DNs to radiance with bias and gain values, which is specific to a given individual scene. The second step involves the conversion of radiance to ToA reflectance. Landsat 8 OLI sensor is more sensitive than the TM and ETM+, hence the data can be rescaled to 16 – bits DNs which ranges between 0 and 65536.

2.5 Pre – processing

In this study, the images of Landsat 7 *TM*, 7 *ETM+* and 8 OLI were imported and then introduced into the ERDAS Imagine software, from the GEOTIFF formats. It was then stacked into layers (bands) which was converted to IMG format. The scenes are then clipped from which the area of interest (AOI) is achieved and then geo – registered to obtain the (UTM Zone 32N) coordinate system. Overlay and image differencing operations are observed to ascertain for change analysis through differencing of the respective images pairs. Cross tab was also performed to determine the unique combinations of value in two qualitative images. SAVI values is then achieved in the images using ArcGIS 10.5 software.

2.6 Determination of the Soil Adjusted Vegetation Index (SAVI)

Here, the raster calculator in ArcGIS 10.4 software was used. The soil adjusted vegetation index (SAVI) method highlight areas where the vegetative cover is low and where soil surface is bare. The index was automatically extracted from the satellite imagery. For Landsat sensor *TM* and *ETM+* adopted, the following relations were utilized for SAVI (Alhammadi *et al* 2008).

SAVI = (Float (band 4 – band 3) / (band 4 + band 3 +0.5))*Float (1.5)

For Landsat sensor *OLI*, the following relations were observed.

SAVI = (Float (band 5 – band 4) / (band 5 + band 4 +0.5))*Float (1.5)

Where b4 and b3 denotes the reflectance value of the fourth (the near – infrared band) and third bands (the red band) of the pre – processed images. L is the adjustment factor (value = 0.5)

Fig. 3 depict the methodology flow diagram for the study.

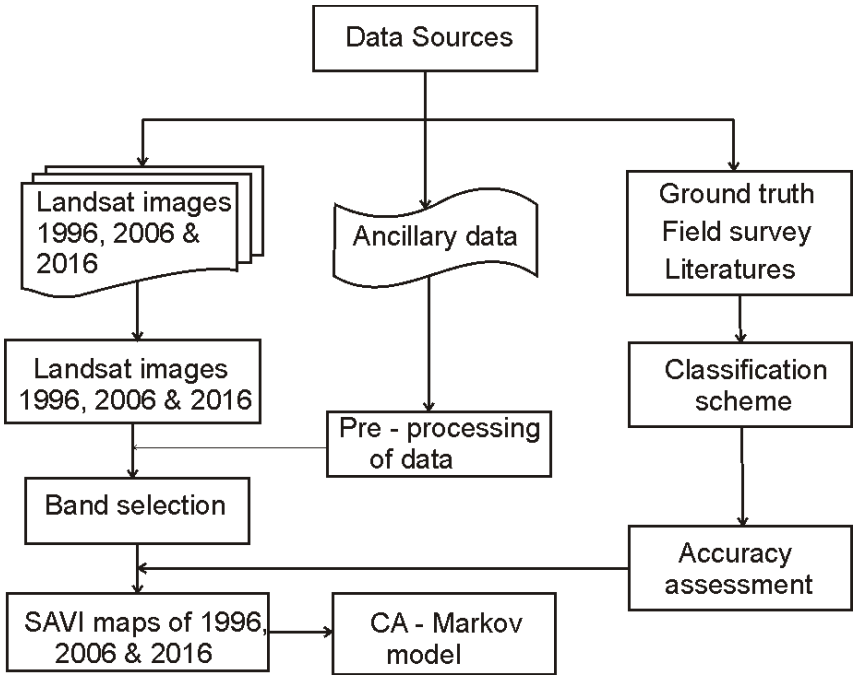

Fig. 3. Methodology flow diagram for the study

Table 1. Image density classification scheme (modified after [39])

Code	Image density classification
1	Low SAVI
2	Moderate SAVI
3	High SAVI

2.7 Image Classification

Image classification involves a process, whereby an image is categorized into few number of individual classes, which is dependence on the reflectance values. The major aim, by which an image is classified, is to delineate information associated with the landscape from the remote sensing satellite data. In this study, the maximum likelihood classification is the classification scheme, adopted by which supervised classification was performed to categorized the satellite data into 3 classes viz Low SAVI, moderate SAVI and high SAVI. False color composite (FCC) maps were produced with the ArcGIS 10.5 software for all the time series study images. The classification process started with obtaining the training samples for the SAVI classes, then the trained samples were evaluated using statistical analysis. Signature file were created using the trained samples, and then the classification analysis observed. The classified maps were finally superimposed to produce the final output classified SAVI maps for the study.

2.7.1 Development of image classification scheme

The overall objective of performing image classification is to position all image pixels within an image and to prepare the classification scheme. Sequel to the prior knowledge obtained about the study area couple with reconnaissance survey and knowledge gained from previous research, a general classification scheme is developed and modified after [39]. For the study, the image density classification scheme is shown in Table 1 and identified with codes 1, 2 and 3 which represent low, moderate and high SAVI image density classification classes.

2.8 Change Rate Analysis

To determine the change area for the study, the SAVI 1996 image was subtracted from the SAVI 2006 image. Likewise, the SAVI 2006 image was also subtracted from the SAVI 2016 image and finally, the SAVI 1996 image is also subtracted from the SAVI 2016 image. The arithmetic for the change area is calculated as follows: DSAVI = SAVI (2006) – SAVI (1996); DSAVI = SAVI (2016) – SAVI (2006) DSAVI = SAVI (2016) – SAVI (1996).

3. RESULTS AND INTERPRETATION

The result show that hydrocarbon micro - seepage has a considerable effect on the soil and sediment within the study area. Considering the result for the maximum value, the SAVI increased from – 0.580 in 1996 to – 0.230 in 2006 and then decreases to – 0.564 in 2016. Similarly, the minimum value of the SAVI increases from 0.130 in 1996 to 1.490 in 2006 and then decreases to – 0.105 in 2016. Fig. 7 depict the statistics of the SAVI images over the study periods. Changes associated with the SAVI values in the study, is due to the influence of the various anthropogenic activities.

The output SAVI maps for the study is depict in Figs. 4 – 6 with the descriptive statistics shown in Fig. 7.

3.1 Savi Image Classification

Table 2 depict the SAVI density classes for the study. The results shows that the values were designated into low, moderate and high areas, to show the effect of hydrocarbon micro - seepage on soil, for the three epoch study years. Figs. 8 – 10 shows that SAVI density classification cover class for the study, with the descriptive statistics shown in Fig. 11. Within the study, the category of high SAVI density classification was observed to increase progressively from 26.13*km* (31.95%) in 1996 to 28.56 *km* (34.92%) in 2006 and then to 30.07 *km* (36.77%) in 2016. The moderate SAVI density reduce from 33.15*km* (40.53%) in 1996 to 31.70 *km* (36.77%) in 2006 and then to 28.59 *km* (34.96%) in 2016 while the category of low SAVI density decrease from 22.50*km* (27.51%) in 1996 to 21.51 *km* (26.31%) in 2006 and then increase to 23.11 *km* (28.26%) in 2016.

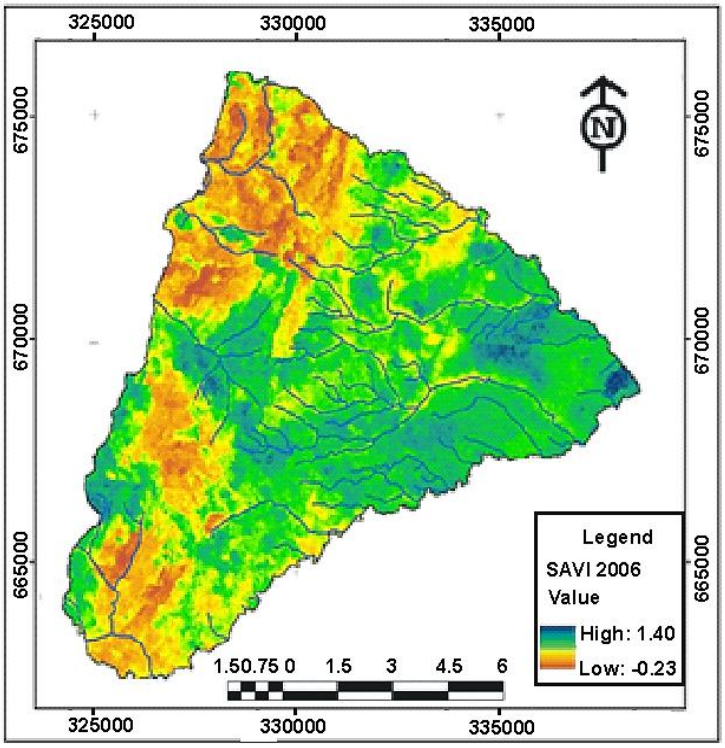

Fig. 4. SAVI map for Landsat *TM* (1996)

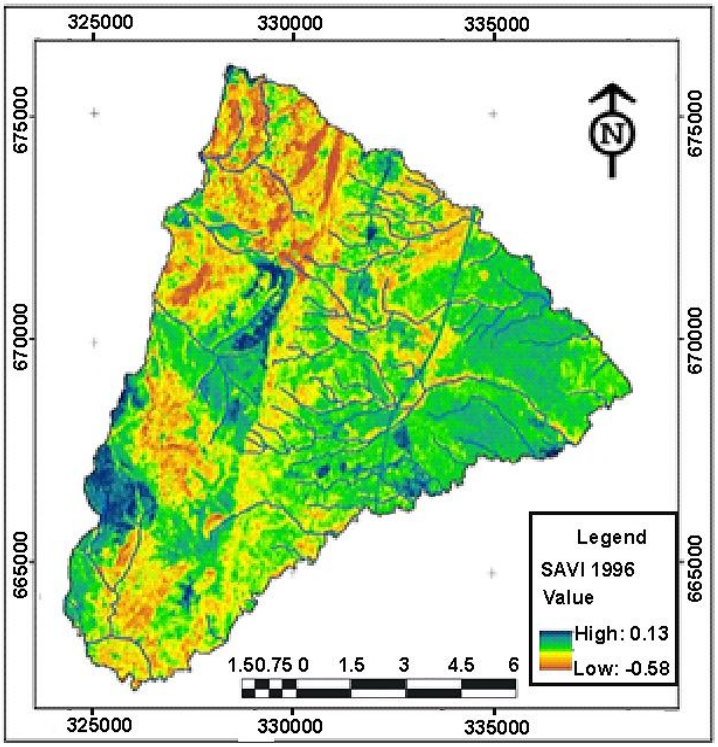

Fig. 5. SAVI map for Landsat *ETM+* (2006)

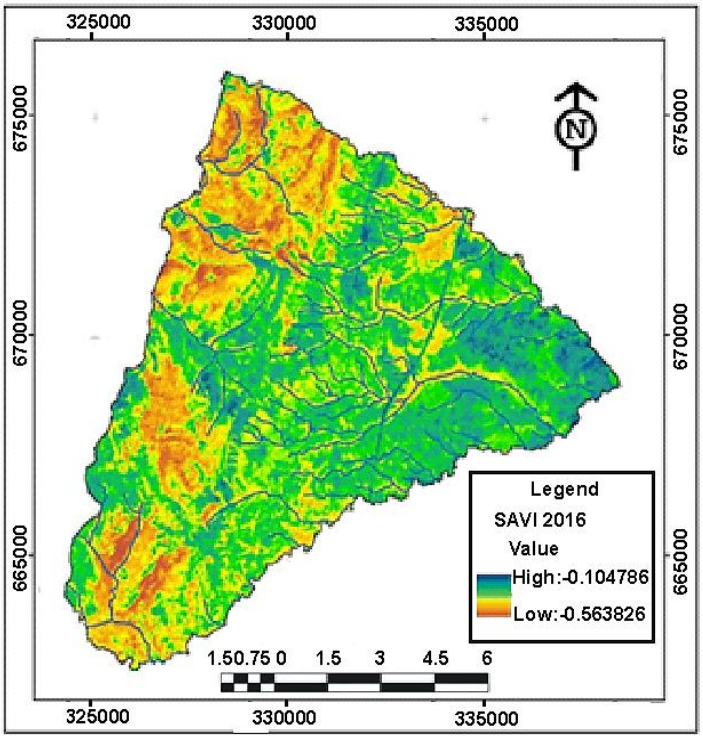

Fig. 6. SAVI map for Landsat *OLI* (2016)

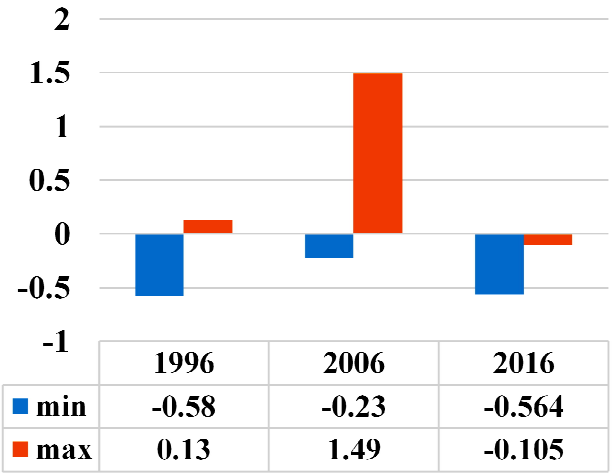

Fig. 7. Descriptive statistics for SAVI values

Table 2. SAVI density classification

Classes Cover	1996		2006		2016	
	Area (Km^2)	(%)	Area (Km^2)	(%)	Area (Km^2)	(%)
Low	22.4991	27.51	21.5154	26.31	23.1147	28.26
Moderate	33.1488	40.53	31.7034	38.77	28.5930	34.96
High	26.1324	31.95	28.5615	34.92	30.0726	36.77
Total	**81.7803**	**100**	**81.7803**	**100**	**81.7803**	**100**

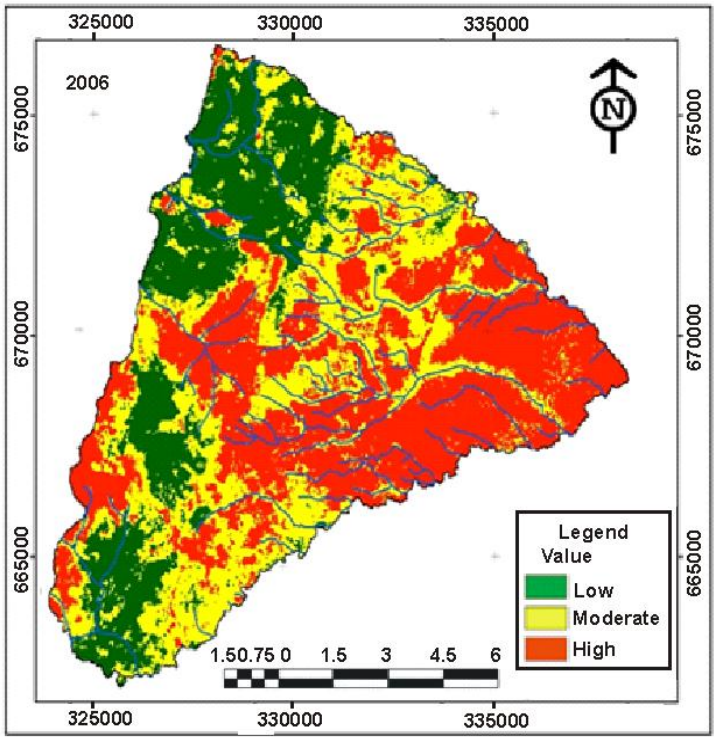

Fig. 8. SAVI density classification cover class Map for Landsat *TM* (1996)

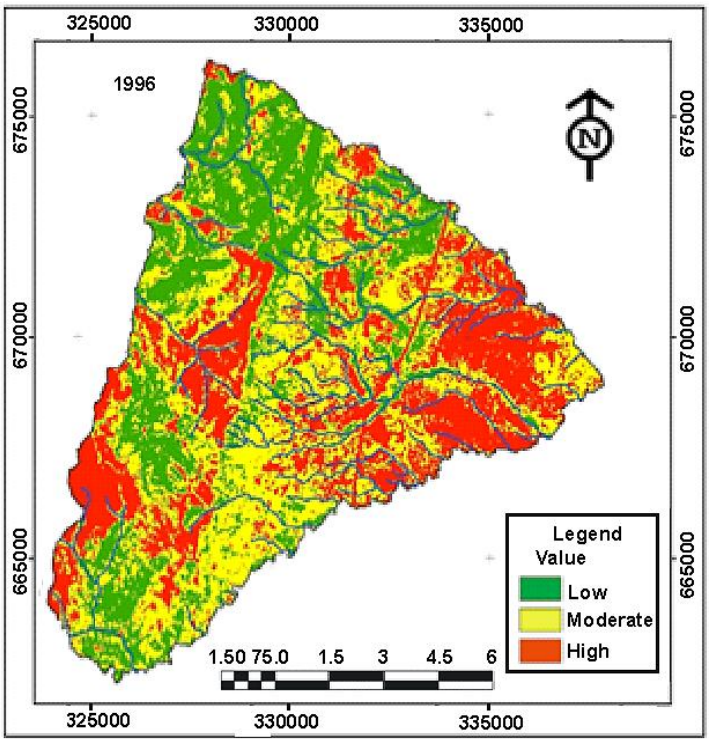

Fig. 9. SAVI density classification cover class map for Landsat *ETM+* (2006)

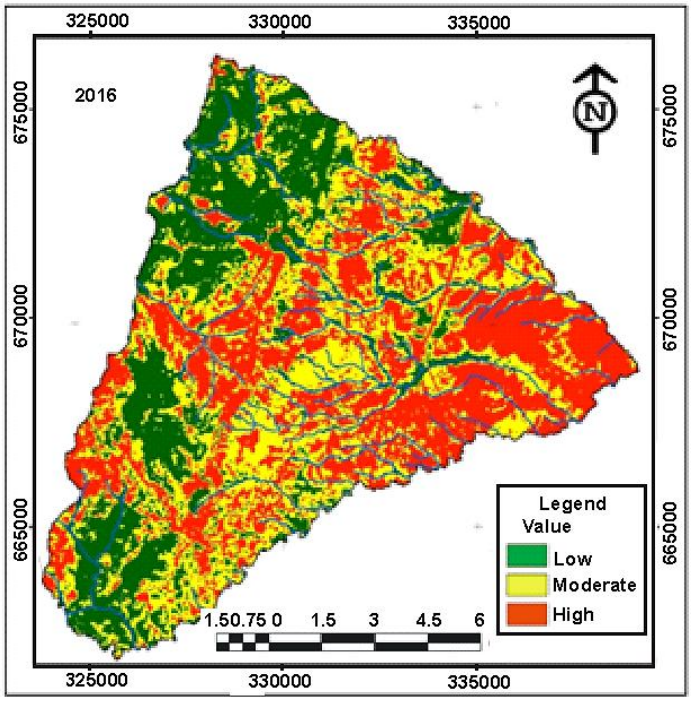

Fig. 10. SAVI density classification cover class density Map for Landsat *OLI* (2016)

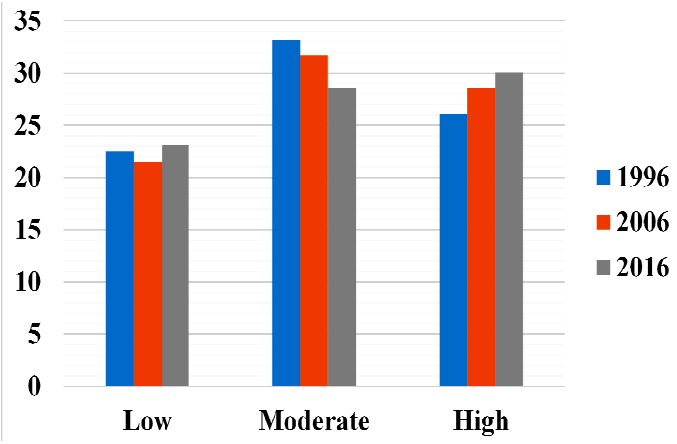

Fig. 11. Descriptive statistics for SAVI classification

3.2 Overlay Operation and Magnitude of SAVI Changes

Overlay operation involves considering two or more different thematic maps, which are of the same study area and overlying them to form a composite new layer [4]. In this study, the different classified maps were overlaid, to generate a visual presentation of the areal extent of changes, which have occurred within the period of the study for the SAVI. Here, the overlay operations was observed to ascertain the amount of changes determined. The SAVI model was categorized into three classes viz increase, decrease and unchanged for the Landsat imageries change which occurred between (Landsat *TM* 1996 and Landsat *ETM*+ 2006); (Landsat *ETM* + 2006 and Landsat *OLI* 2016) and (Landsat *TM* 1996 and Landsat *OLI* 2016) respectively. Table 3 depicts a complete table for the magnitude of SAVI changes for the study.

Table 3. Magnitude of SAVI changes

S/N	SAVI Categories	Change btw (1996 – 2006)		Change btw (2006 – 2016)		Change btw (1996 – 2016)	
		Area (km^2)	(%)	Area (km^2)	(%)	Area (km^2)	(%)
1	Un – changed	12.3201	15.06	17.1405	20.96	13.5045	16.51
2	Decreased	39.8925	48.78	40.4514	49.46	51.5205	63.00
3	Increased	29.5677	36.16	24.1884	29.58	16.7553	20.49
	Total	**81.7803**	**100**	**81.7803**	**100**	**81.7803**	**100**

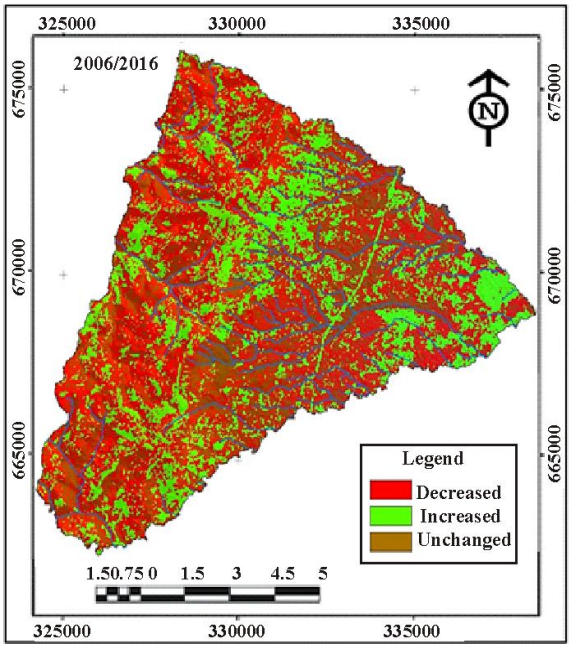

Fig. 12. Magnitude of SAVI Changes map for Landsat TM/OLI (1996/2006)

Figs. 12 – 14 depicts the output maps of the magnitude of SAVI changes, during the study. Here, the generated change are produced by combining the multi – temporal imagery of Landsat SAVI. Fig. 12 shows the output map for the changes which have occurred in the study between (1996 – 2006), while Figs. 13 and 14 highlight the respective output maps for the changes, which occurs between (2006 – 2016) and (1996 – 2016) respectively. By visualizing the SAVI maps, it is of the view that most areas have light brown colors, hence depicting no change category, since each of the pixel exhibit the same value in each band. Areas with the red and green color highlight "decrease and increase category" of SAVI respectively.

3.3 Image Differencing for Savi Change Detection

Image differencing is an important technique when studying change detection [4]. The method is observed by subtracting the respective digital number (DN) value of one pixel for a given band from another DN value, both are of the same pixel for the same band of another date. Image differencing can be positive or negative. A positive image differencing shows an increase in the value of class size, while a decrease in class size shows a negative value. An image difference with value "zero" highlight a constant figure in the class size. In this study, two different classified images (1996 and 2006); (2006 and 2016) and (1996 and 2016) were compared, in order to identify areas, which is distinctly different in the brightness values. The new image formed represent change produced, by considering the differences between the respective images. Table 4 depict the descriptive of the image differences while Figs. 16 – 18 shows the output maps for the respective image differencing for the study for classified images (1996/2006); (2006/2016) and (1996/2016).

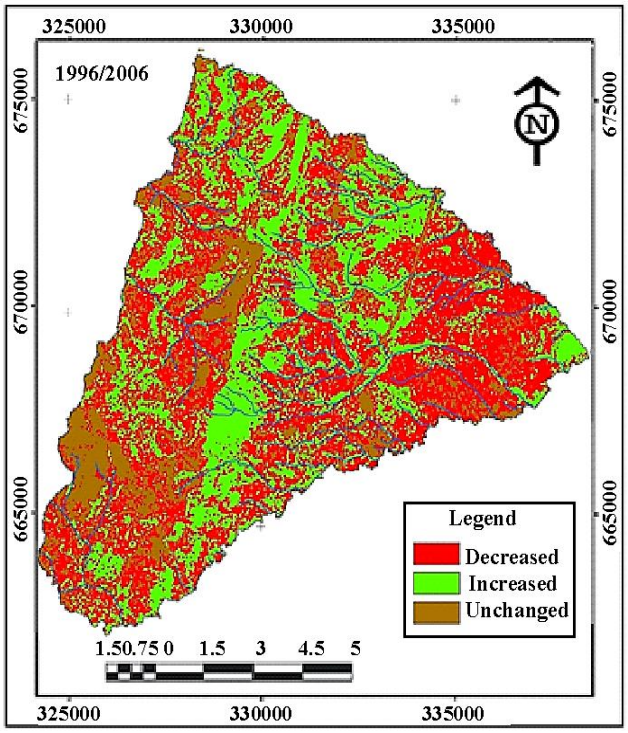

Fig. 13. Magnitude of SAVI Changes map map Landsat *ETM+/OLI* (2006/2016)

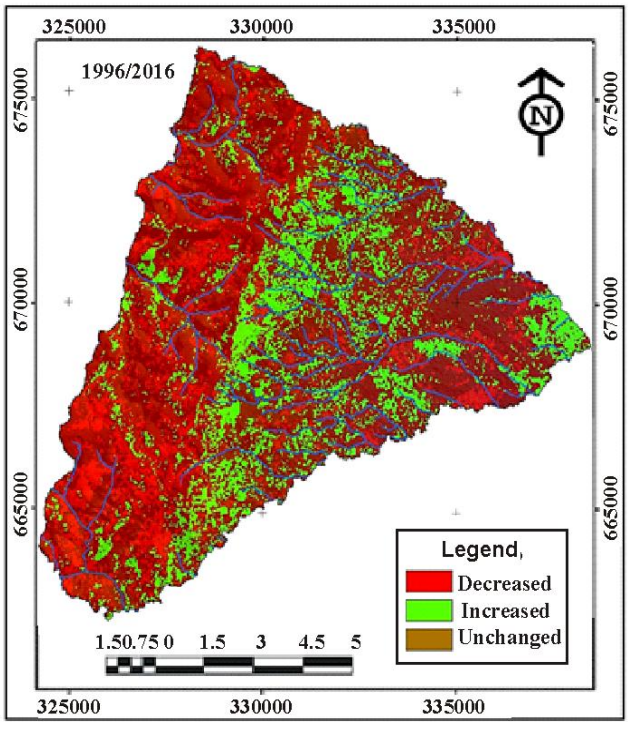

Fig. 14. Magnitude of SAVI Changes map for Landsat *TM*/*OLI* (1996/2016)

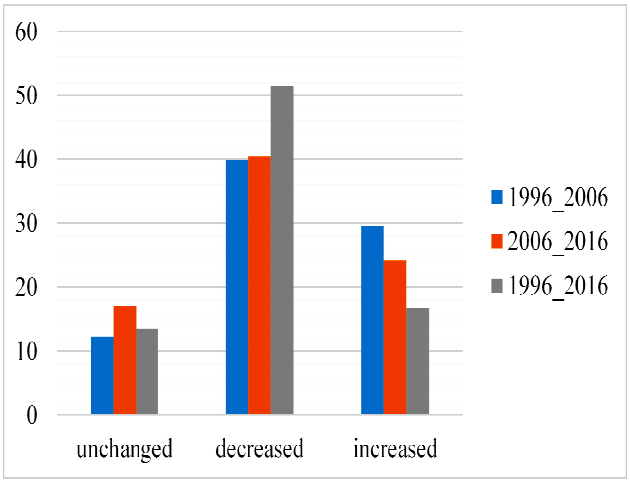

Fig. 15. Descriptive statistics for the magnitude of the SAVI change

Table 4. Descriptive of the Image Differences

	Image Differences (1996/2006)	Image Differences (2006/2016)	Image Differences (1996/2016)
Values	**Area (km^2)**	**Area (km^2)**	**Area (km^2)**
- 2	0.6624	0.5624	0.7613
- 1	12.8412	11.5613	13.3467
0	134.91	127.53	131.57
1	16.02	15.12	14.11
2	0.7344	0.6513	0.6713

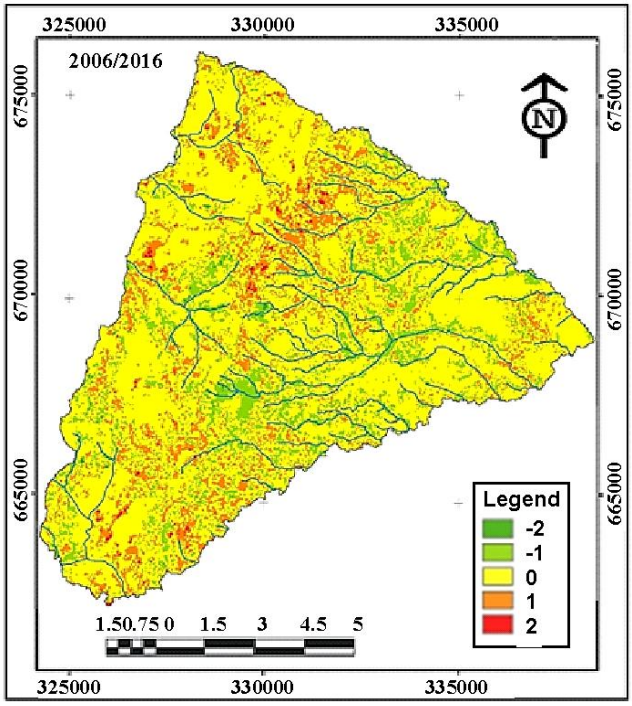

Fig. 16. Image Difference between map Landsat *TM/OLI* (1996/2006)

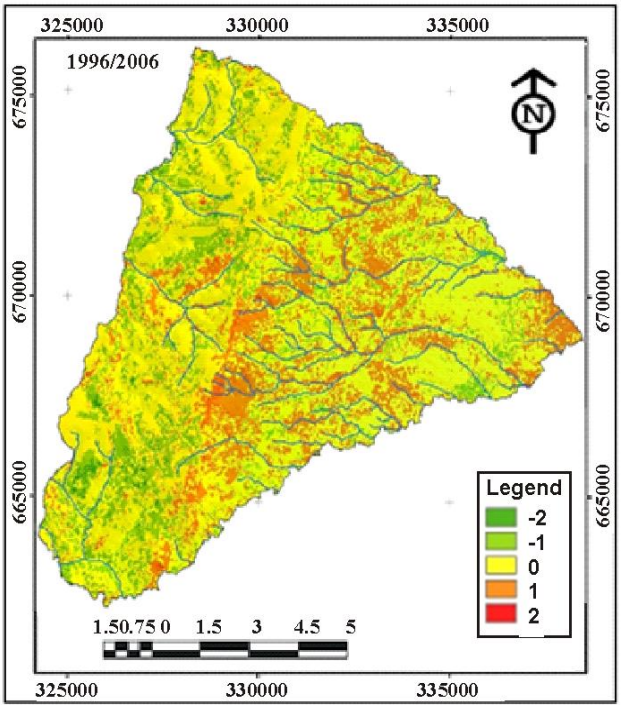

Fig. 17. Image Difference between map Landsat *ETM+/OLI* (2006/2016)

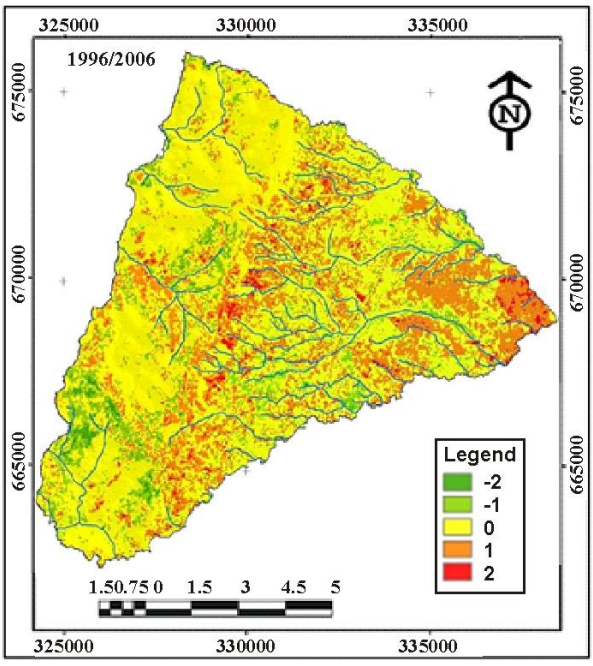

Fig. 18. Image Difference between map for Landsat *TM*/*OLI* (1996/2016)

3.4 Transition Probability Matrix

Transition Probability Matrix highlight the fact that the probability of one classification class will change to the other category. This matrix is prepared by multiplying each column in the transition probability matrix. For a 3 by 3 matrix table, the rows denotes older classification class

while the column is the newer categories. In the study, the transition probability matrix is prepared between different image classifications for 1996 against 2006; 2006 against 2016 and 1996 against 2016. A chi – square and degree of freedom statistics is adopted and a significance of the Cramer's V is tested. Kappa measure of association is adopted as 2 images with exactly the same number of categories is adopted. The overall Kappa analysis for each respective maps are 0.2469, 0.7757 and 0.7235. Tables 5-7 expound the transition probability matrix for 1996 (column) against 2006 (rows); transition probability matrix for 2006 (column) against 2016 (rows) and the transition probability matrix for 1996 (column) against 2016 (rows).

3.4.1 Transition probability matrix of 1996 (columns) against 2006 (rows)

Here, the row categories represent SAVI classes in 1996 while the column shows the 2006 classes. Following from Table 5, the Low SAVI has 16958 probability of remaining Low SAVI and 6391 of a change to the moderate SAVI in 2006. This shows a change (reduction) with probability of change, which is higher than its stability. Moderate SAVI exhibit the highest class with 19571 probability of remaining moderate SAVI in 2006. High SAVI also exhibit probability which is as high 20335 value in order to remain as high SAVI in 2006, hence signifying stability.

Table 5. Transition matrix table 1996 (columns) against 2006 (rows)

	1	2	3	Total
1	16,958	6,391	93,212	116,561
2	7,511	19,571	8,144	35,226
3	530	10,870	20,335	31,735
Total	**24,999**	**36,832**	**121,691**	**183,522**

Chi Square	=	275723.93750
df	=	12
P-Level	=	0.0000
Cramer's V	=	0.7077
Overall Kappa	=	0.2469

Table 6. Transition matrix table 2006 (columns) against 2016 (rows)

	1	2	3	Total
1	19,473	6,012	198	25,683
2	4,100	20,135	7,535	31,770
3	24,002	9,079	92,988	126,069
Total	**47,575**	**35,226**	**100,721**	**183,522**

Chi Square	=	314147.40625
df	=	9
P-Level	=	0.0000
Cramer's V	=	0.7554
Overall Kappa	=	0.7757

Table 7. Transition matrix table 1996 (columns) against 2016 (rows)

	1	2	3	Total
1	6,141	18,267	7,362	31,770
2	817	11,659	20,938	33,414
3	737	6,906	110,695	118,338
Total	**7,695**	**36,832**	**138,995**	**183,522**

Chi Square	=	277594.50000
df	=	12
P-Level	=	0.0000
Cramer's V	=	0.7101
Overall Kappa	=	0.7235

3.4.2 Transition probability matrix of 2006 (columns) against 2006 (rows)

In Table 6, the row categories highlight the SAVI classes in 2006 while the column depicts the 2016 classes. Thus, the Low SAVI has 19,473 probability of remaining Low SAVI and 6012 of a change to the moderate SAVI in 2016. This indicate a change, which reduces with probability of change, which is higher than its stability. Moderate SAVI express the highest class with 20,135 probability of remaining moderate SAVI in 2016. High SAVI shows 92,988 to remain high SAVI in 2016, whereby it implies stability.

Table 8. Transition matrix table between 1996/2006; 2006/2016 and 1996/2016

Tabulation between 1996/2006				Tabulation between 2006/2016			Tabulation between 1996/2016		
Category	Km^2	Legend		Category	Km^2	Legend	Category	Km^2	Legend
1	18.3015000	3	3	0.0000000	0	0	16.2360000	1	1
2	15.2622000	1	1	17.5257000	1	1	6.2154000	2	1
3	5.7519000	2	1	5.4108000	2	1	0.6624000	3	1
4	0.5013000	3	1	0.1782000	3	1	18.8451000	15	1
5	6.7599000	1	2	3.6900000	1	2	5.5269000	1	2
6	17.6139000	2	2	18.1215000	2	2	16.4403000	2	2
7	7.3296000	3	2	6.7815000	3	2	6.6258000	3	2
8	0.0009000	0	3	0.2997000	1	3	0.0009000	0	3
9	0.4761000	1	3	8.1711000	2	3	0.7344000	1	3
10	9.7830000	2	3	21.6018000	3	3	10.4931000	2	3

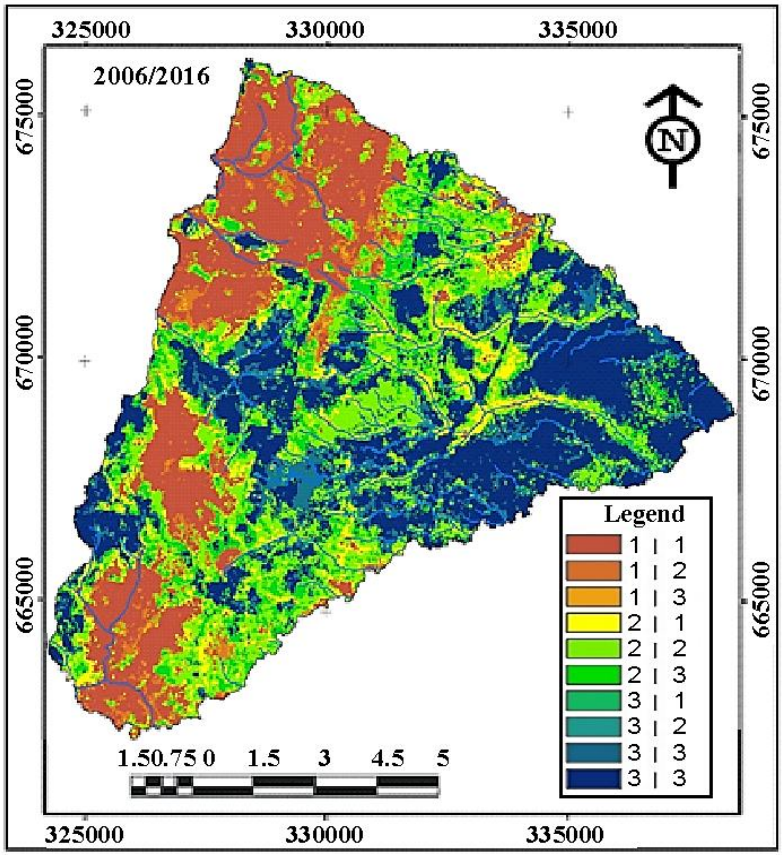

Fig. 19. Transition matrix map for Landsat *TM/ETM+* (1996/2006)

3.4.3 Transition probability matrix of 1996 (columns) against 2016 (rows)

Here, the row categories show that the SAVI classes in 1996 with the column categories showing the 2016 classes. From Table 7, we see that the Low SAVI has 6,141 probability of remaining Low SAVI and 18,267 of a change to the moderate SAVI in 2016. This indicate an increase in the change with probability of change, which is higher than its stability. Moderate SAVI exhibit a class with 11,659 probability of remaining moderate SAVI in 2016. High SAVI express probability with high 110,695 value in order to remain as high SAVI in 2016, hence signifying stability.

Table 8 shows the overall transition matrix table from 1996 – 2016 for the study.

Figs. 19 – 21 shows the transition matrix output maps for the study.

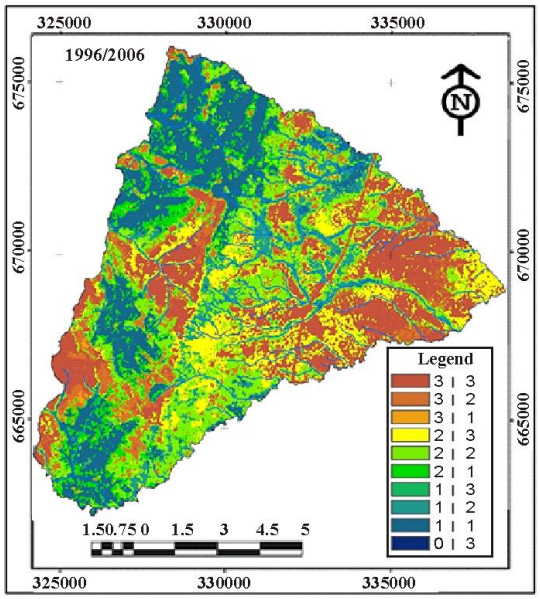

Fig. 20. Transition matrix map for Landsat *ETM+/OLI* (2006/2016)

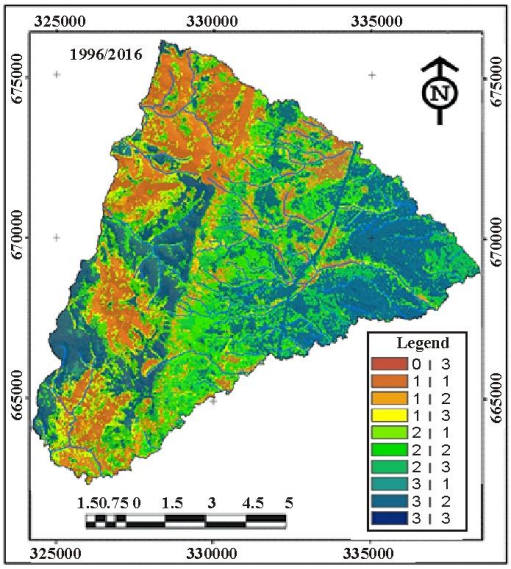

Fig. 21. Transition matrix map for Landsat *TM*/*OLI* (1996/2016)

Table 9. Projected SAVI analysis for 2030

SAVI Classes	2030	
	Area (Km^2)	Percentage (%)
Low	25.7607	30.77
Moderate	14.173	16.93
High	43.7926	52.30

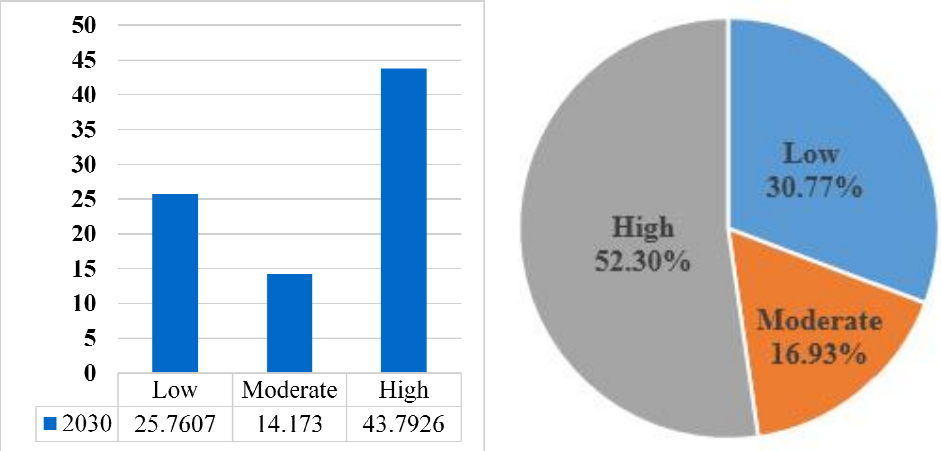

Fig. 22. Descriptive statistics for SAVI density classification for 2030

4. THE SOIL ADJUSTED VEGETATION INDEX (SAVI) MODELLING AND PREDICTION FOR 2030

The Markov Chain Analysis is an excellent tool for modelling land use changes. A Markovian process is express as one, by which the future state of a particular system is modeled mainly on immediately preceding state. Markovian chain analysis highlight land use and classification changes from one state to another based for project future change. This is obtained by preparing a transition probability matrix of respective land use change from a particular period of time to another, which highlight the state of occurring changes. The transition probability might be accurate, with basis on per category analysis, but no knowledge about the spatial distribution of the occurrences taking place within each of the land use category. Owing to this, the Cellular Automata (CA) is used, so as to include the spatial character to the model. The CA – Markov utilizes the output which is derived from the Markov Chain Analysis, most particularly the Transition Area file, so as to apply a contiguity filter. The CA often develop a spatial explicit weighting which is heavy in areas that proximate to existing like land classification classes. Table 9 shows the overall projected SAVI classification results for the 2030. Here, the SAVI classification for low, moderate and high class values are 25.76 km^2, 14.17 km^2 and 43.79 km^2 respectively representing 30.77%, 16.93% and 52.30%. When compared to the SAVI analysis for 2016, we see that the category of low SAVI increase in 2030, decrease in the moderate category and increase again in the high SAVI category class.

Fig. 22 show the descriptive statistics SAVI output maps for the study for 2030.

5. CONCLUSION

Remote Sensing have proven to be an excellent tool in mapping and modelling areas, associated with hydrocarbon micro – seepage. In the study, Landsat satellite imageries were utilized to monitor the influence of hydrocarbon micro - seepage, by producing different SAVI classification maps. The findings of the study shows that the high SAVI density classification increased progressively from 31.95% to 34.92% and to 36.77% in 1996, 2006 and 2016 respectively. The category of moderately SAVI density classification reduced from 40.53% in 1996 to 38.77% in 2006 and then to 36.96% in 2016 while the category of low SAVI density was found to decrease progressive from 27.51% in 1996 to 26.31% in 2006 and then increased to

28.26% in 2016. The SAVI model is categorized into increase, decrease and unchanged classes, with the un – changed category increasing from 12.32km^2 (15.06%) in 1996 to 17.17 km^2 (20.96%) in 2006 and then decelerate to 13.50 km^2 (16.51%) in 2016. The decrease category changed from 39.89km^2 (48.78%) in 1996 to 40.45 km^2 (49.45%) in 2006 and to 51.52 km^2 (63.0%) in 2016 while the increase category changed from 29.57km^2 (36.16%) in 1996 to 24.18 km^2 (29.58%) in 2006 and to 16.75 km^2 (20.49%) in 2016. Image differencing, cross tabulation and overlay operations were various techniques performed in the study, to ascertain the effect of hydrocarbon micro - seepage. The Markov chain analysis is a technique which was used to predict the effect of the hydrocarbon micro - seepage in the study for 2030.The study shows that SAVI is an excellent remote sensing techniques for mapping areas influenced by hydrocarbon micro – seepage.

COMPETING INTERESTS

Authors have declared that no competing interests exist.

REFERENCES

1. Shi PL, Fu BH, Ninomiya Y. Detecting lithologic features from ASTER VNIR-SWIR multispectral data in the arid region: A case study in the eastern Kalpin uplift, southwest Tian Shan. Chinese Journal of Geology. 2010;45(1):333-347.
2. Donovan T, Forgey R, Roberts A. Aeromagnetic detection of diagenetic magnetite over oil fields. American. Association of Petroleum Geology; Bulletin. 1979;63:245-248.
3. Segal D, Merin I. The use of Landsat Thematic Mapper data for mapping hydrocarbon microseepage induced mineralogic alteration, Lisbon Valley, Utah. Journal of Photogrammetric Engineering and Remote Sensing. 1989;4:1137-1145.
4. Schumacher D. Hydrocarbon-induced alteration of soils and sediments. American Association of Petroleum Geologists, Memoir. 1996;66:71-89.
5. Van der Meer FD, Van Dijk P, Van der Werff H. Remote Sensing and Petroleum Seepage: A Review and Case Study. Terra Nova. 2020;14(1):1–17.
6. Rasiah V, Voroney RP, Groenevelt PH, Kachanoski RG. Modifications in soil water retention and hydraulic conductivity by an oily waste. Soil Technology. 1990;3:367-372.
7. Anoliefo GO, DE Vwioko. Effects of lubricating oil on the growth of Capsicum annum L. and Lycopersicon esculentum Miller. Environment Pollution. 1995;88:361-364.
8. Noomen MF. Hyperspectral reflectance of vegetation affected by underground hydrocarbon seepage. PhD thesis, ITC; 2007.
9. Hanson RS, Hanson TE. Methanotrophic bacteria. Microbiological Review. 1996;60(2):439-471.
10. White DC. Hyperspectral remote sensing of canopy scale vegetation stress associated with buried gas pipelines: Published Doctor of Philosophy thesis, Newcastle University. 2007;306.
11. Schumacher D, Abrams MA. Hydrocarbon Migration and its Near-Surface Expression: American Association of Petroleum Geologists, Memoir. 1996;66:445.
12. Saunders D, Burson K, Thompson C. Model for hydrocarbon microseepage and related nearsurface alterations. AAPG Bulletin. 1999;83:170–185.
13. Petroleum Safety Authority. Trends in Risk Level – Land Facilities in the Norwegian Petroleum Activities; 2011.
14. Teeuw RM. Mapping Hazardous Terrain using Remote Sensing. Geological Society, London, Special Publications. 2007;283.
15. NTSB. Natural gas exploitation and fire in South Riding, Virginia, National Transportation Safety Board, Washington, DC, Technical Report; 2001.
16. NTSB. Natural gas pipeline rupture and fire near Carlsbad, New Mexico. National Transportation Safety Board, Washington, DC, Technical Report; 2003.
17. Schumacher DD. Surface geochemical exploration for oil and gas: New life for an old technology, TLE; 2000.
18. Drew MC. Plant injury and adaptation to oxygen deficiency in the root environment: a review. Plant and Soil. 1983;75:179–199.
19. Pysek P, Pysek A. Changes in vegetation caused by experimental leakage of natural gas: Remote sensing of environment. 1989;29:193–204.
20. Serrano A, Gallego M, Gonazalez L, Tejada M. Natural attenuation of diesel aliphatic hydrocarbons in contaminated agriculture soil: Environmental Pollution. 2008;494–502.

21. Cloutis E. Spectral reflectance properties of hydrocarbons: remote-sensing implications. Science. 1989;245:165–168.
22. Horig B, Kuhn F, Oschu TF, Lehmann F. Hymap hyper-spectral remote sensing to detect hydrocarbons. International Journal of Remote Sensing. 2001;22:1413–1422.
23. Li L, Ustin S, Lay M. Application of AVIRIS data in detection of oil-induced vegetation stress and cover change at Jornada, New Mexico. Remote Sensing of Environment. 2005;94:1–16.
24. Orlov DS, Ammosova MI, Bocharnikova EA. Remote monitoring of oil – populated soils using soil reflectance spectra: Optical monitoring of the environment. 1993;321–325.
25. Schumacher D. Surface geochemical exploration for petroleum. American Association of Petroleum Geologists, Treatise of Petroleum Geology Handbook. 1999;18-27.
26. Kuhn F, Oppermann K, Horig B. Hydrocarbon Index – an algorithm for hyperspectral detection of hydrocarbons: International Journal of Remote Sensing. 2004;2467-2473.
27. Zirnig W, Hausamann D, Schreier G. Utilizing High Resolution Remote Sensing Used to Monitor Natural Gas Pipelines. Earth Observation Magazine. 2002;11:9.
28. Alhammadi MS, Glenn EP. Detecting date palm trees health and vegetation greenness change on the eastern coast of the United Arab Emirates with SAVI: International Journal of Remote Sensing. 2008;29:1745–1765.
29. Schultz GA, Engman ET. Remote Sensing in Hydrology and Water Management, Springer, Heidelberg, Germany; 2000.
30. Turner DP, Cohen WB, Kennedy RE, Fassnacht KS, Briggs JM. Relationships between Leaf Area Index and LANDSAT TM Spectral Vegetation Indices across Three Temperate Zone Sites: Remote Sensing of Environment. 1999;70:52–68.
31. Spencer CH, Spry KE. A comparison of Slope-Based Vegetation Indices for agricultural applications; 1996. Available:http://www.biogeorecon.com /vegindcs.htm
32. Gibson PJ, Power CH, Goldin SE, Rudahl KT. Introductory to Remote Sensing: Digital Image process and applications. 2000;111-113.
33. National Population Commission of Nigeria; 2006.
34. Nigerian Voice (TNV) Newspaper; 2012.
35. Daniel O, Chinenye O. Water Quality Assessment of Ugwueme Surface and Ground Water System: International Journal of Science and Research (IJSR). 2017;6(9):833 – 838.
36. Okpala-Okaka C, Igbokwe JI. Revision of Nsukka N.E topographic map sheet 287 1:50,000 (1964) using Nigeria SAT-1 imagery. Nigerian Journal of Space Research. 2010;7:13-24.
37. Ugo Chukwu I. Subsurface Evaluation of source rock and hydrocarbon potential of the Anambra Basin, South Eastern Nigeria. Dissertation. 2010;3-4.
38. United States Geological Survey (USGS). Landsat, the band designations for the Landsat satellites; 2016. Available:http://landsat.usgs.gov/band_des ignations_landsat_satellites.php
39. Anderson et al. A Land Use and Land Cover Classification System for Use with Remote Sensor Data. Geological Survey Professional Paper No. 964, U.S; 1976.

Peer-review history:
The peer review history for this paper can be accessed here:
http://www.sdiarticle4.com/review-history/61263